# Rabi-resonant and intraband transitions in a multilevel quantum dot system controlled by the cavity-photon reservoir and the electron-photon coupling

Nzar Rauf Abdullah[a,b,c]

[a] *Division of Computational Nanoscience, Physics Department, College of Science, University of Sulaimani, Sulaimani 46001, Kurdistan Region, Iraq*
[b] *Komar Research Center, Komar University of Science and Technology, Sulaimani 46001 Kurdistan Region, Iraq*
[c] *Science Institute, University of Iceland, Dunhaga 3, IS-107 Reykjavik, Iceland*

## ARTICLE INFO

## ABSTRACT

The transport properties of a wire-dot system coupled to a quantized single photon with linear polarization in a 3D-cavity is theoretically studied using a quantum master equation. The system is also coupled to a photon reservoir, environment. We interplay between the electron-photon coupling, $g_\gamma$, and the cavity-reservoir coupling, $\kappa$, in three cases: $\kappa < g_\gamma$, $\kappa = g_\gamma$, and $\kappa > g_\gamma$. The current peaks due to intraband transitions between the Rabi-resonant states are formed when the electron-photon coupling is dominant, $\kappa < g_\gamma$. The broadening of the current peaks depends on the photon polarization and the geometry of the resonant states. It is remarkable that a current plateau is found when $\kappa \geq g_\gamma$ in which the cavity-reservoir is dominant. In this case, the intraband transitions are diminished and the current peaks are not seen.

## 1. Introduction

To understand the quantum nature of light-matter interaction, one may choose the combination of a nanoelectronic system and a cavity QED among several techniques [1,2].The most desirable nanoelectronic system for such studies is the quantum dot (QD) with two-level [3] or multi-level energy [4]. The two-level QDs strongly coupled to a cavity lead to the Rabi oscillations that can be controlled by the electric field in the cavity. This has applications in quantum computing [5], quantum communication networks [6], and creating single photon sources [7,8] in which the single photon is used to manage optical quantum simulators [9,10], multi-qubit gates [11], and other physical phenomena in nanodevices [12–15]. Furthermore, the multi-level QDs coupled to a cavity can be used for switching [16] and lasing [17] processes.

Two physical parameters are generally considered in studying the light-matter interaction which are the electron-photon coupling, $g_\gamma$, and the cavity-reservoir coupling, $\kappa$. One can compare these two parameters to see the system in either strong or weak coupling regime [18]. The system is said to be the strong-coupling regime if the cavity-reservoir coupling is smaller than the electron-photon coupling, $\kappa < g_\gamma$. In such systems, a vacuum Rabi splitting is exceeded [19], and the charge qubit decoherence rate and the vacuum Rabi mode splitting are resolved [20]. In the weak coupling regime, $\kappa \geq g_\gamma$, the spontaneous emission rate is calculated and shown that the QD radiative lifetime is modified [21].

The electron transport properties through a QD coupled to a photon field is another interested area of the light-matter interaction in which the transported electron can be controlled by the photon field [22,23]. The current peaks due to Rabi splitting of a QD under the influences of photon are observed and the system can be used to measure photo-luminescence [24], electroluminescence [25,26]. Furthermore, the photon-induced transport through Rabi-splitting states [27], and entanglement characteristics of a photon source with an electronic system [28] are observed.

Based on the information given by the aforementioned studies, we model a quantum dot embedded in a quantum wire and coupled to a 3D-cavity and the photon reservoir, environment. In addition, the wire-dot system is connected to two electron reservoirs or leads. The characteristics of electron transport under the quantized photon field is investigated using a Markovian master equation [29–31]. We model the QD system in response to the optimism that conductance and electron transport will be studied soon in the conduction band of a GaAs heterostructure [32]. They claim that the two-dimensional electron gas in a GaAs heterostructure is very appropriate to study intersubband transitions under the influence of cavity-photon. In addition, experiments with similar system coupled to external leads are underway [33]. In our published works, the properties of electron transport in the transient and the stead state regimes are reported in which the photon-assisted transport [34], thermoelectric transport [35–37], and Rabi-oscillations [38] are found. In the current paper, the transport of

current through a wire-dot system in steady state is reported in three different regimes: $\kappa < g_\gamma$, $\kappa = g_\gamma$, and $\kappa > g_\gamma$. It is observed that the photon replica states formed in the presence of the cavity actively contribute to the electron transport when $\kappa < g_\gamma$. As a result, the Rabi-splitting are seem to be strong which in turn the resonant current peaks are raised. In contrast, when $\kappa \geqslant g_\gamma$, the resonant current peaks are not seen, instead of them a current plateau is noticed.

The rest of the paper is demonstrated as follows. We show the model system in Sec. 2. Results are discussed for the model in Sec. 3. Finally, we have our conclusion in Sec. 4.

## 2. Theoretical formalism

The system under investigation is a QD with diameter $d \simeq 66.5$ nm embedded in a quantum wire with length $L_x = 150$ nm. We assume the quantum wire is two-dimension with hard-wall and parabolic confined in the x- and y-direction, respectively [39]. The QD system and the leads are made of GaAs material. The wire-dot system is coupled to a quantized photon field in a 3D-cavity, and the cavity is also coupled to a photon reservoir or environment. We let the photons in the cavity to be polarized in either x- or y-direction.

The Hamiltonian of the wire-dot system with the photon cavity can be written as [40–42,31]

$$H_S = H_{W-QD} + H_{Zee} + H_\gamma + H_{e-\gamma}. \tag{1}$$

Herein, $H_{W-QD}$ is the Hamiltonian of the wire-dot system which is given by

$$H_{W-QD} = \sum_i \ (E_i + eV_g) d_i^\dagger d_i + \frac{1}{2} \sum_{iji'j'} \ V_{int} d_i^\dagger d_j^\dagger d_{j'} d_{i'}, \tag{2}$$

where $E_i$ is the energy of a single-electron (SE) state, $V_g$ is the gate voltage that is electrostatic potential moving the energy states of the wire-dot system with respect to the chemical potential of the electron reservoirs or the leads, and

$$V_{int} = \langle ij|V_{e-e}|i'j' \rangle$$
$$= \int d\mathbf{r} d\mathbf{r'} \psi_i^S(\mathbf{r})^* \psi_j^S(\mathbf{r'})^* V\left( \mathbf{r} - \mathbf{r'} \right) \psi_{i'}^S\left( \mathbf{r'} \right) \psi_{j'}^S(\mathbf{r}) \tag{3}$$

are the Coulomb interaction matrix elements in the single-electron state basis with $\psi^S(\mathbf{r})$ being the SE state wavefunctions, the Coulomb interaction potential $V(\mathbf{r} - \mathbf{r'})$, and $d_i^\dagger$ ($d_i$) being the electron creation (annihilation) operator of the QD system. An exact diagonalization method is utilized to solve the Coulomb interacting ME Hamiltonian for the wire-dot system [43].

The exact-diagonalization technique in the single-electron state basis is also used to obtain the SE energy state, $E_i$, shown in Eq. (2) [44]. The second term of Eq. (1) is the Zeeman Hamiltonian, $H_{Zee} = g\mu_B B\sigma_z/2$ where $g$ is tensorial effective Land g-factor and $\mu_B$ refers to the Bohr magneton, $B$ is the weak external magnetic field, and $\sigma_z$ indicates Pauli matrices.

The third term of Eq. (1), $H_\gamma = \hbar\omega_\gamma \hat{a}^\dagger \hat{a}$, defines the quantized photon field where $\hbar\omega_\gamma$ is the photon energy and $\hat{a}^\dagger$ and $\hat{a}$ are the creation and annihilation operators of the photon field in the cavity, respectively. The last term in Eq. (1), $H_{e-\gamma}$, is the electron-photon coupling Hamiltonian

$$H_{e-\gamma} = g_\gamma \sum_{ij} \ d_i^\dagger d_j \, g_{ij} \{a + a^\dagger\}$$
$$+ \frac{g_\gamma^2}{\hbar\Omega_w} \sum_i \ d_i^\dagger d_i \left[ \widehat{N}_\gamma + \frac{1}{2}(a^\dagger a^\dagger + aa + 1) \right] \tag{4}$$

where the first term of Eq. (4) is called paramagnetic and the second term is diamagnetic Hamiltonian that demonstrate the electron-photon interaction with $g_{ij}$ [30] the dimensionless electron-photon coupling factor, and $\widehat{N}_\gamma$ the photon number operator. The electron-photon

coupling strength is defined by $g_\gamma = eAa_w \Omega_w/c$, where $a_w$ refers to the effective magnetic length, $e$ is the electron charge, and $\Omega_w$ displays the effective confinement frequency of electrons in the QD system which is obtained via $\Omega_w = \sqrt{\Omega_0^2 + \omega_c^2}$ with $\Omega_0$ the electron confinement frequency due to the lateral parabolic potential, and $\omega_c$ being the cyclotron frequency due to the external magnetic field.

The dimensionless electron-photon coupling tensor of the electrons to the 3D-cavity can be defined by

$$g_{ij} = \frac{a_w}{2\hbar} \int d\mathbf{r} \left[ \psi_i^S(\mathbf{r})^* \{(\hat{\mathbf{e}} \cdot \boldsymbol{\pi}) \psi_j^S(\mathbf{r})\} \right.$$
$$\left. + \{(\hat{\mathbf{e}} \cdot \boldsymbol{\pi}) \psi_i^S(\mathbf{r})\}^* \psi_j^S(\mathbf{r}) \right], \tag{5}$$

where $\boldsymbol{\pi}$ is the sum of the momentum operator of an electron and vector potential of the external magnetic field [45], and $\hat{\mathbf{e}} = (e_x, 0)((0, e_y))$ demonstrates the electric field that is polarized parallel (perpendicular) to the transport direction.

To see the evolution of the electrons in the system in the steady state regime, we use a Markovian master equation. The projection formalism is used based on the density operator [46,47]. Since we are interested in the state of the central system, QD system after the coupling to the leads, the reduced density operator of the central system is obtained via

$$\hat{\rho}_S = \text{Tr}_{L,R}[\hat{\rho}(t)]. \tag{6}$$

where $\hat{\rho}(t)$ is the density operator of the total system. Here, the trace over the Fock space of the left lead (L) and the right lead (R) is taken into account [48–51]. We are dealing with the long-time evolution and the steady state of the QD system in this study. Therefore, further transform with equation into a corresponding Markovian equation for the reduced density operator of the QD-system gives [29]

$$\partial_t \hat{\rho}_S(t) = -\frac{i}{\hbar}[\widehat{H}_S, \hat{\rho}_S(t)] - \{\Lambda^L[\hat{\rho}_S; t] + \Lambda^R[\hat{\rho}_S; t]\}$$
$$- \frac{\kappa}{2\hbar}(\bar{n}_R + 1)\{2\alpha\hat{\rho}_S\alpha^\dagger - \alpha^\dagger\alpha\hat{\rho}_S - \hat{\rho}_S\alpha^\dagger\alpha\}$$
$$- \frac{\kappa}{2\hbar}(\bar{n}_R)\{2\alpha^\dagger\hat{\rho}_S\alpha - \alpha\alpha^\dagger\hat{\rho}_S - \hat{\rho}_S\alpha\alpha^\dagger\}. \tag{7}$$

where $\Lambda^L$ and $\Lambda^R$ indicate the "dissipation" processes caused by both leads [38] which are governed by

$$\Lambda^l\left[ \rho_S; t \right] = \frac{1}{\hbar^2} \int d \in D^l(\epsilon)\theta(t)\{[\tau^l, \Omega[\rho_S]] + \text{h. c.}\}. \tag{8}$$

Herein, $D^l(\epsilon)$ is the density of state of the $l$ lead, $\theta(t)$ indicates the Heaviside unit step function, $\tau^l$ displays the many-body version of the coupling tensor of lead $l$, and $\Omega[\rho_S]$ is the time integral [52].

The current from the left lead into the QD-system, $I_L^c$, and the current from it into the right lead, $I_R^c$, can be defined as

$$I_{L,R}^c = \text{Tr}_S(\Lambda^{L,R}[\hat{\rho}_S; t]Q). \tag{9}$$

where $Q = -e \sum_i d_i^\dagger d_i$ is the charge operator of the wire-QD system with $\hat{d}^\dagger$ ($\hat{d}$) the electron creation (annihilation) operator of the wire-QD system, respectively.

Another interested physical parameter is the average total number of photons in the cavity which can be calculated as

$$N_\gamma = \text{Tr}_S(\hat{\rho}_S a^\dagger a), \tag{10}$$

where $a^\dagger$ ($a$) are the photon creation and annihilation operators, respectively.

## 3. Results

In this section, the main interested results are presented. The chemical potential of the left and the right leads are assumed to be $\mu_L = 1.65$ meV and $\mu_R = 1.55$ meV, respectively. Furthermore, for the sake of avoiding the strong Lorentz force on the charge of system, we consider a weak external magnetic, $B = 0.1$ T [42]. The QD system is
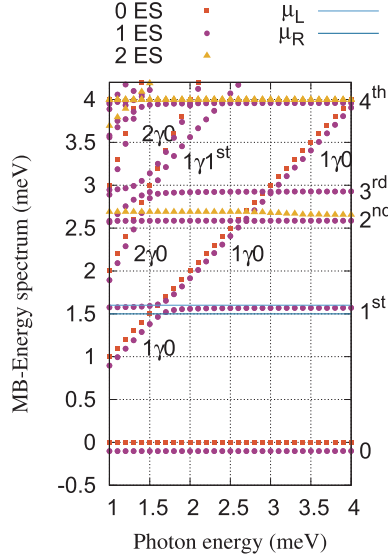
**Fig. 1.** Energy spectrum or Many-Body (MB) energy spectrum of the QD system coupled to the photon cavity as a function of the photon energy with $x$-polarized photon field, where 0ES (red squares), 1ES (purple circles), 2ES (brown triangles) stand for zero-electron states, are one-electron states, and two-electron states, respectively. 0, 1st, 2nd, 3rd, and 4th are the one-electron ground-state, first-, second-, third-, fourth-excited state, respectively. In addition, $1\gamma0$ and $2\gamma0$ indicate the one- and two-photon replica of the 0, and the $1\gamma1^{st}$ is the one-photon replica state of the $1^{st}$. The electron-photon coupling strength $g_\gamma = 0.1$ meV, $\kappa = 10^{-4}$, and $n_R = 1$. Other constant parameters are $\mu_L = 1.65$ meV (light blue line) and $\mu_R = 1.55$ meV (dark blue line), $B = 0.1$ T, $eV_g = 0.651$ meV, $T_{L,R} = 0.5$ K and $\hbar\Omega_0 = 2.0$ meV. (For interpretation of the references to colour in this figure legend, the reader is referred to the web version of this article.)

also coupled to a quantized photon filed confined in a cavity with a single photon mode and the cavity is coupled to a photon reservoir, the environment. The mean photon number of the photon reservoir is assumed to be $n_R = 1$ in this study.

### 3.1. x-Polarized photons

Herein, we let the photon field to be polarized in the $x$-direction, i.e., the photon field in the cavity is in the same direction of electron motion in the wire-dot system. Fig. 1 shows the energy spectrum of the wire-dot system coupled to a photon field with $x$-polarization. By changing the photon energy, anti-crossings in the energy spectrum are found at the photon energies 1.7 between the one-photon replica of the ground state, $1\gamma0$, and the first-excited state $1^{st}$, 2.7 between $1\gamma0$ and the second-excited state, $2^{nd}$, and 3.4 meV between the one-photon replica of the first-excited state, $1\gamma1^{st}$, and sixth-excited state, $6^{th}$ (not shown). The photon-exchange between some of these anti-crossings states indicates that the anti-crossings states are the Rabi-resonant states [39].

Fig. 2 demonstrates the current going from the left lead to the QD system, $I_L^c$, as a function of the photon energy for the $x$-polarized of the photon field. The current going from the wire-dot system to the right lead, $I_R^c$, has the same characteristics of the $I_L^c$ because the system is the steady state regime. We present the current of the system for three different cases: $\kappa < g_\gamma$ (purple squares), $\kappa = g_\gamma$ (green triangles), and $\kappa > g_\gamma$ (blue diamonds). In the first case, when the electron-photon coupling, $g_\gamma$, is greater than the cavity-reservoir coupling, $\kappa$, three current peaks are found corresponding to the Rabi-resonant states shown in Fig. 1. The interaction between the electrons and the photon in cavity is dominant leading to the strong intraband transition between the corresponding Rabi-resonant states. As a result, a high current is raised which in turn the current peaks are seen.

Increasing the cavity-reservoir coupling, $\kappa$, in a way that $\kappa = g_\gamma$ or
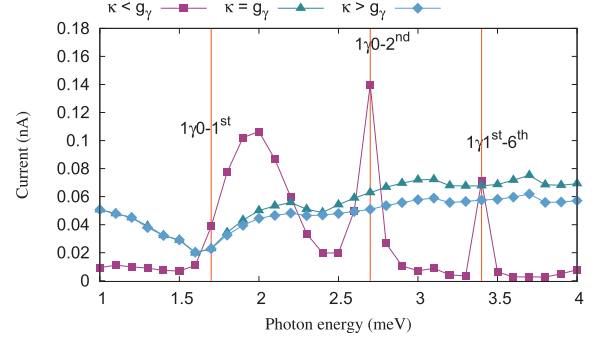


**Fig. 2.** Current as a function of the photon energy for $\kappa = 10^{-4} < g_\gamma$ (purple squares), $\kappa = 0.1 = g_\gamma$ (green triangles), and $\kappa = 0.3 > g_\gamma$ (blue diamonds) in the $x$-polarized of the photon field. The vertical lines (red) display the location of the main resonance states. Other constant parameters are $g_\gamma = 0.1$ meV, $n_R = 1$, $\mu_L = 1.65$ meV, $\mu_R = 1.55$ meV, $B = 0.1$ T, $eV_g = 0.651$ meV, $T_{L,R} = 0.5$ K, and $\hbar\Omega_0 = 2.0$ meV. (For interpretation of the references to colour in this figure legend, the reader is referred to the web version of this article.)

$\kappa > g_\gamma$ the current peaks are diminished and a current plateau is observed. The reason is that the intraband transition between the Rabi-resonant states are reduced at the high cavity-reservoir coupling, $\kappa \geqslant g_\gamma$. To further explain it, we present the average total number of photons in the cavity (a) and the occupation of the wire-dot system (b) in Fig. 3.

In the case of $\kappa < g_\gamma$ (purple squares), the mean photon number is decreased at the Rabi-resonant places indicating that the photon is absorbed by the electrons in the lower states and transfer them to the higher states, intraband transitions. As a result, the mean photon
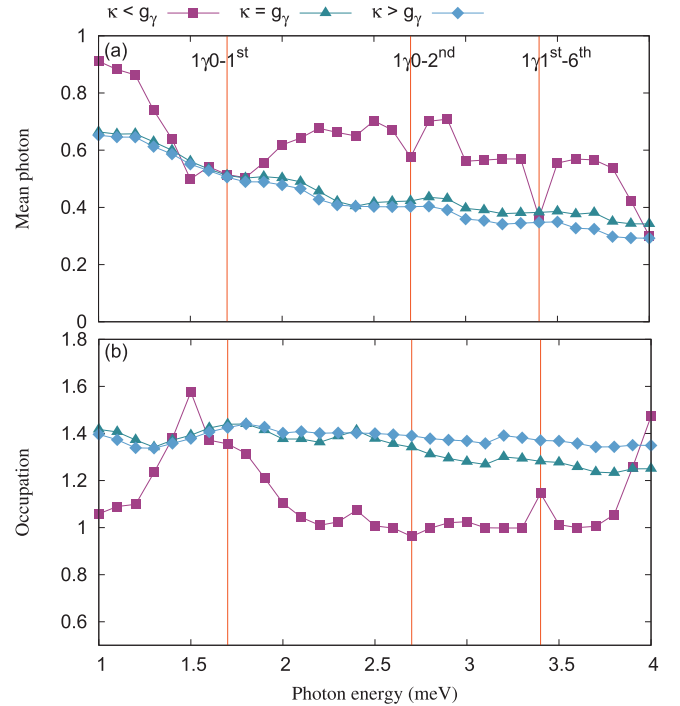


**Fig. 3.** Mean photon number (a) and occupation (b) versus the photon energy for $\kappa = 10^{-4} < g_\gamma$ (purple squares), $\kappa = 0.1 = g_\gamma$ (green triangles), and $\kappa = 0.3 > g_\gamma$ (blue diamonds) in the $x$-polarized of the photon field. The vertical lines (red) display the location of the main resonance states. Other constant parameters are $g_\gamma = 0.1$ meV, $n_R = 1$, $\mu_L = 1.65$ meV, $\mu_R = 1.55$ meV, $B = 0.1$ T, $eV_g = 0.651$ meV, $T_{L,R} = 0.5$ K, and $\hbar\Omega_0 = 2.0$ meV. (For interpretation of the references to colour in this figure legend, the reader is referred to the web version of this article.)
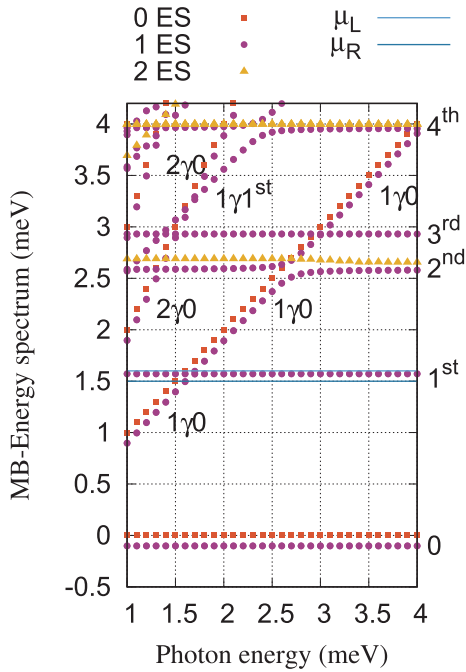
**Fig. 4.** Energy spectrum or Many-Body (MB) energy spectrum of the QD system coupled to the photon cavity as a function of the photon energy with $y$-polarized photon field, where 0ES (red squares), 1ES (purple circles), 2ES (brown triangles) stand for zero-electron states, are one-electron states, and two-electron states, respectively. 0, 1st, 2nd, 3rd, and 4th are the one-electron ground-state, first-, second-, third-, fourth-excited state, respectively. In addition, $1\gamma0$ and $2\gamma0$ indicate the one- and two-photon replica of the 0, and the $1\gamma1^{st}$ is the one-photon replica state of the $1^{st}$. The electron-photon coupling strength $g_\gamma = 0.1$ meV, $\kappa = 10^{-4}$, and $n_R = 1$. Other constant parameters are $\mu_L = 1.65$ meV (light blue line) and $\mu_R = 1.55$ meV (dark blue line), $B = 0.1$T, $eV_g = 0.651$ meV, $T_{L,R} = 0.5$ K and $\hbar\Omega_0 = 2.0$ meV. (For interpretation of the references to colour in this figure legend, the reader is referred to the web version of this article.)

number in the cavity decreases at the Rabi-resonant condition. On the other hand the occupation of the system is enhanced at the location of the Rabi-resonances showing that the corresponding resonant states are occupied at each Rabi-resonant condition. Increasing the cavity-photon reservoir, $\kappa \gtrsim g_\gamma$ (green rectangles and blue diamonds), plateau in both the mean photon number and the occupation is found indicating that the intraband transition between the Rabi-resonant states are diminished. As a result a plateau in the current is seen as it was shown in Fig. 2.

### 3.2. y-Polarized photons

In this section, we demonstrate the properties current transport of the QD system coupled to a cavity with $y$-polarized photon field. Fig. 4 shows the energy spectrum of the wire-dot system as a function of the photon energy. It is clearly seen that the Rabi-splitting between $1\gamma0$ and $1^{st}$ at the photon energy 1.7 meV is smaller than that of the $x$-polarization. In contrast, the Rabi-splitting between $1\gamma0$ and $2^{nd}$ at the photon energy 2.7 meV is larger than that of the $x$-polarization shown in Fig. 1. This is due to the fact that some states are more polarizable in the $x$-direction and some other states in the $y$-direction [39]. We should mention that the photon-exchange between the resonant states is stronger for the larger Rabi-splitting.

Fig. 5 displays the current going from the left lead to the wire-dot system, $I_L^c$, as a function of the photon energy. In the case of $\kappa < g_\gamma$ (purple squares), three current peaks are observed at the Rabi-resonant places shown in Fig. 4, just like it was seen for the $x$-polarization. The broadening of the leftmost current peak has been found to decrease
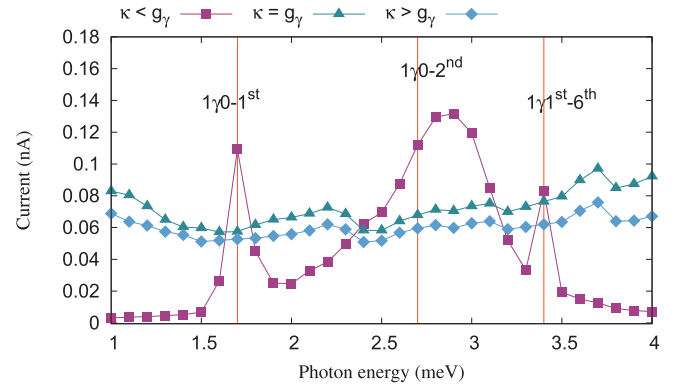


**Fig. 5.** Current as a function of the photon energy is plotted for $\kappa = 10^{-4} < g_\gamma$ (purple squares), $\kappa = 0.1 = g_\gamma$ (green triangles), and $\kappa = 0.3 > g_\gamma$ (blue diamonds) in the $y$-polarized of the photon field. The vertical lines (red) indicates the location of the main resonance states. Other parameters are $g_\gamma = 0.1$ meV, $n_R = 1$, $\mu_L = 1.65$ meV, $\mu_R = 1.55$ meV, $B = 0.1$T, $eV_g = 0.651$ meV, $T_{L,R} = 0.5$ K, and $\hbar\Omega_0 = 2.0$ meV. (For interpretation of the references to colour in this figure legend, the reader is referred to the web version of this article.)

because the Rabi-splitting between $1\gamma0$ and $1^{st}$ at photon energy 1.7 meV is smaller in the $y$-polarization comparing to the $x$-polarized of the photon field. In contrast, the middle current peak is more broader here comparing to the $x$-polarization. The reason is that the Rabi-splitting is large between $1\gamma0$ and $2^{nd}$ at the photon energy 2.7 meV in the $y$-polarization [16].

In other two cases, $\kappa = g_\gamma$ (green triangles) and $\kappa > g_\gamma$ (blue diamonds), very slow oscillations in the current and very small current peaks are found at the Rabi-resonant states with a shift in the peaks. In
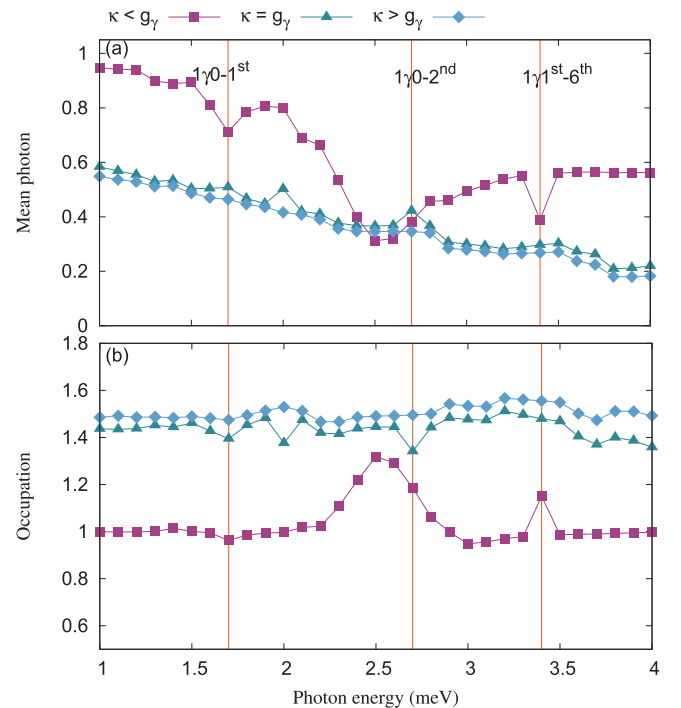


**Fig. 6.** Mean photon number (a) and occupation (b) as a function of the photon energy are plotted for $\kappa = 10^{-4} < g_\gamma$ (purple squares), $\kappa = 0.1 = g_\gamma$ (green triangles), and $\kappa = 0.3 > g_\gamma$ (blue diamonds) in the $y$-polarized of the photon field. The vertical lines (red) demonstrate the location of the main resonance states. Other parameter are $g_\gamma = 0.1$ meV, $n_R = 1$. $\mu_L = 1.65$ meV, $\mu_R = 1.55$ meV, $B = 0.1$T, $eV_g = 0.651$ meV, $T_{L,R} = 0.5$ K, and $\hbar\Omega_0 = 2.0$ meV. (For interpretation of the references to colour in this figure legend, the reader is referred to the web version of this article.)

Fig. 6, we present the mean photon (a) and the occupation (b) of the system as a function of the photon energy. A suppression in the mean photon number and enhancement in the occupation confirm the strong intraband transition between the Rabi-resonant states in the case of $\kappa < g_\gamma$ (purple squares). Furthermore, slow oscillations in the mean photon number and the occupation in the case of $\kappa = g_\gamma$ (green triangles) and $\kappa > g_\gamma$ (blue diamonds) indicate the weak intraband transition between the corresponding Rabi-resonant states.

## 4. Conclusion

We have studied the characteristics of electron transport through a wire-dot system coupled to two electron reservoirs or leads using a Markovian master equation. The wire-dot system is also coupled to a cavity and the photon reservoir in which the exact diagonalization technique is used to treat the electron-electron and electron-photon interactions in the system. We interplay the electron-photon coupling and the cavity-reservoir coupling to control peaks in the current that are formed due to the intraband transitions of the Rabi-resonant states. When the electron-photon coupling is dominant, the strong intraband transitions are observed and the current peaks remain strong. In contrast, if the cavity-reservoir coupling is stronger than the electron-photon coupling, the intraband transitions become weak and a plateau in the current is seen. Our study may be beneficial for the filed of quantum information processes in which the Rabi-resonant effect plays an important role [53,54].

## Author statement

1. We state that the intraband transitions can be used to investigate quantum information. 2. The intraband transitions can be found in the strong coupling regime.

## Declaration of Competing Interest

The authors declare that they have no known competing financial interests or personal relationships that could have appeared to influence the work reported in this paper.

## Acknowledgment

## Appendix A. Supplementary data

Supplementary data associated with this article can be found, in the online version, at https://doi.org/10.1016/j.rinp.2019.102686.

## References

[1] Langford NK, Sagastizabal R, Kounalakis M, Dickel C, Bruno A, Luthi F, Thoen DJ, Endo A, DiCarlo L. Nat Commun 2017;8:1715.
[2] Cottet A, Kontos T, Douot B. Phys Rev B 2015;91. 205417.
[3] Vora PM, Bracker AS, Carter SG, Sweeney TM, Kim M, Kim CS, Yang L, Brereton PG, Economou SE, Gammon D. Nat Commun 2015:article.
[4] Madsen KH, Lehmann TB, Lodahl P. Phys Rev B 2016;94. 235301.
[5] Frisk Kockum A, Miranowicz A, De Liberato S, Savasta S, Nori F, Reviews Nature. Physics 2019;1:19.
[6] De Greve K, Yu L, McMahon PL, Pelc JS, Natarajan CM, Kim NY, Abe E, Maier S, Schneider C, Kamp M, Hofling S, Hadfield RH, Forchel A, Fejer MM, Yamamoto Y. Nature 2012;491:421.
[7] Imamoglu A, Yamamoto Y. J Phys Rev Lett 1994;72:210.
[8] Giannelli L, Schmit T, Calarco T, Koch CP, Ritter S, Morigi G. New J Phys 2018;20. 105009.
[9] Aspuru-Guzik A, Walther P. Nat Phys 2012;8. 285 EP, review Article.
[10] Cialdi S, Rossi MAC, Benedetti C, Vacchini B, Tamascelli D, Olivares S, Paris MGA. Appl Phys Lett 2017;110. https://doi.org/10.1063/1.4977023. 081107.
[11] Lin Q, He B. Sci Rep 2015;5. 12792 EP, article.
[12] Hummer T, Garc'ia-Vidal FJ, Mart'in-Moreno L, Zueco D. Phys Rev B 2013;87. 115419.
[13] Delbecq MR, Bruhat LE, Viennot JJ, Datta S, Cottet A, Kontos T. Nat Commun 2013;4:1400. article.
[14] S'anchez R, Platero G, Brandes T. J Phys Rev B 2008;78:125308.
[15] Kreinberg S, Grbesic T, Strauss M, Carmele A, Emmerling M, Schneider C, Hofling S, Porte X, Reitzenstein S. Light: Sci Appl 2018;7:41.
[16] Kim N-C, Ko M-C. Plasmonics 2015;10:605.
[17] Karlewski C, Heimes A, Schon G. Phys Rev B 2016;93. 045314.
[18] Snijders HJ, Frey JA, Norman J, Flayac H, Savona V, Gossard AC, Bowers JE, van Exter MP, Bouwmeester D, Loffler W. J Phys Rev Lett 2018;121. 043601.
[19] Bruhat LE, Cubaynes T, Viennot JJ, Dartiailh MC, Desjardins MM, Cottet A, Kontos T. Phys Rev B 2018;98. 155313.
[20] Stockklauser A, Scarlino P, Koski JV, Gasparinetti S, Andersen CK, Reichl C, Wegscheider W, Ihn T, Ensslin K, Wallraff A. J Phys Rev X 2017;7. 011030.
[21] Englund D, Fattal D, Waks E, Solomon G, Zhang B, Nakaoka T, Arakawa Y, Yamamoto Y, Vukovi J. Phys Rev Lett 2005;95. 013904.
[22] Kibis OV. J Phys Rev Lett 2011;107. 106802.
[23] Gudmundsson V, Sitek A, Lin P-Y, Abdullah NR, Tang C-S, Manolescu A. ACS Photon 2015;2:930.
[24] Leng H, Szychowski B, Daniel M-C, Pelton M. Nat Commun 2018;9:4012.
[25] Cirio M, De Liberato S, Lambert N, Nori F. Phys Rev Lett 2016;116. 113601.
[26] Gudmundsson V, Abdulla NR, Sitek A, Goan H-S, Tang C-S, Manolescu A. Ann Phys 2018;530:1700334.
[27] Faraon A, Fushman I, Englund D, Stoltz N, Petroff P, Vuckovic J. Nat Phys 2008.
[28] Eichler C, Lang C, Fink JM, Govenius J, Filipp S, Wallraff A. Phys Rev Lett 2012;109. 240501.
[29] Jonsson TH, Manolescu A, Goan H-S, Abdullah NR, Sitek A, Tang C-S, Gudmundsson V. Comput Phys Commun 2017;220:81.
[30] Gudmundsson V, Jonasson O, Tang C-S, Goan H-S, Manolescu A. Phys Rev B 2012;85. 075306.
[31] Abdullah NR, Tang CS, Manolescu A, Gudmundsson V. J Phys: Condens Matter 2013;25. 465302.
[32] Zhang Q, Lou M, Li X, Reno JL, Pan W, Watson JD, Manfra MJ, Kono J. Nat Phys 2016;12. 1005 EP.
[33] Cottet A, Dartiailh MC, Desjardins MM, Cubaynes T, Contamin LC, Delbecq M, Viennot JJ, Bruhat LE, Douccot B, Kontos T. J Phys: Condens Matter 2017;29. 433002.
[34] Abdullah NR, Tang CS, Manolescu A, Gudmundsson V. Physica E 2014;64:254.
[35] Abdullah NR, Tang C-S, Manolescu A, Gudmundsson V. ACS Photon 2016;3:249. https://doi.org/10.1021/acsphotonics.5b00532.
[36] Abdullah NR, Tang CS, Manolescu A, Gudmundsson V. J Phys: Condensed Matter 2015;27. 015301.
[37] Abdullah NR, Tang C-S, Manolescu A, Gudmundsson V. Physica E 2017.
[38] Gudmundsson V, Gestsson H, Abdullah NR, Tang C-S, Manolescu A, Moldoveanu V. Beilstein J Nanotechnol 2019;10:606.
[39] Abdullah NR, Tang C-S, Manolescu A, Gudmundsson V. arXiv:1903.03655; 2019.
[40] Arnold T, Tang C-S, Manolescu A, Gudmundsson V. J Opt 2015;17. 015201.
[41] Jonasson O, Tang C-S, Goan H-S, Manolescu A, Gudmundsson V. Phys Rev E 2012;86. 046701.
[42] Abdullah NR, Tang C-S, Manolescu A, Gudmundsson V. J Phys: Condens Matter 2016;28. 375301.
[43] Yannouleas C, Landman U. Rep Prog Phys 2007;70:2067.
[44] Abdullah NR, Tang C-S, Gudmundsson V. Phys Rev B 2010;82. 195325.
[45] Abdullah NR. IEEE J Quantum Electron 2016;52:1.
[46] Zwanzig R. J Chem Phys 1960;33:1338.
[47] Nakajima S. Prog Theor Phys 1958;20:948.
[48] Gudmundsson V, Abdullah NR, Sitek A, Goan H-S, Tang C-S, Manolescu A. Phys Lett A 2018;382:1672.
[49] Lax M. Phys Rev 1963;129:2342.
[50] Gardiner CW, Collett MJ. Phys Rev A 1985;31:3761.
[51] Beaudoin F, Gambetta JM, Blais A. Phys Rev A 2011;84. 043832.
[52] Gudmundsson V, Jonsson TH, Bernodusson ML, Abdullah NR, Sitek A, Goan H-S, Tang C-S, Manolescu A. Annalen der Physik 529, 1600177, https://onlinelibrary.wiley.com/doi/pdf/10.1002/andp.201600177.
[53] Imamoglu A, Awschalom DD, Burkard G, DiVincenzo DP, Loss D, Sherwin M, Small A. Phys Rev Lett 1999;83:4204.
[54] Blais A, Huang R-S, Wallraff A, Girvin SM, Schoelkopf RJ. Phys Rev A 2004;69. 062320.